Direct Observation of Dopant Atom Diffusion in a Bulk Semiconductor Crystal Enhanced by a Large Size Mismatch

Ryo Ishikawa,[1,2,*] Rohan Mishra,[3,1,†] Andrew R. Lupini,[1] Scott D. Findlay,[4] Takashi Taniguchi,[5] Sokrates T. Pantelides,[3,1] and Stephen J. Pennycook[6]

[1]*Materials Science and Technology Division, Oak Ridge National Laboratory, Oak Ridge, Tennessee 37831, USA*
[2]*Institute of Engineering Innovation, University of Tokyo, Bunkyo, Tokyo 113-8656, Japan*
[3]*Department of Physics and Astronomy, Vanderbilt University, Nashville, Tennessee 37235, USA*
[4]*School of Physics, Monash University, Victoria 3800, Australia*
[5]*Advanced Key Technologies Division, National Institute for Materials Science, Tsukuba 305-0044, Japan*
[6]*Department of Materials Science and Engineering, The University of Tennessee, Knoxville, Tennessee 37996, USA*

(Received 30 June 2014; published 6 October 2014)

Diffusion is one of the fundamental processes that govern the structure, processing, and properties of materials and it plays a crucial role in determining device lifetimes. However, direct observations of diffusion processes have been elusive and limited only to the surfaces of materials. Here we use an aberration-corrected electron microscope to locally excite and directly image the diffusion of single Ce and Mn dopants inside bulk wurtzite-type AlN single crystals, identifying correlated vacancy-dopant and interstitial-dopant kick-out mechanisms. Using a 200 kV electron beam to supply energy, we observe a higher frequency of dopant jumps for the larger and heavier Ce atoms than the smaller Mn atoms. These observations confirm density-functional-theory-based predictions of a decrease in diffusion barrier for large substitutional atoms. The results show that combining depth sensitive microscopy with theoretical calculations represents a new methodology to investigate diffusion mechanisms, not restricted to surface phenomena, but within bulk materials.

DOI: 10.1103/PhysRevLett.113.155501 PACS numbers: 61.72.-y, 66.30.-h, 68.37.Ma, 78.55.-m

Perfect crystals are rarely useful for most applications, meaning that they have to be doped with impurities to engineer new and improved properties [1–7]. An important pursuit in materials science and engineering has therefore been to understand the atomic-scale dopant-diffusion mechanisms that govern dopant behavior during processing or heat treatment and determine the lifetimes of devices under any given set of working conditions. The presence of defects and impurities often leads to complicated diffusion mechanisms with competitive energy barriers [8–10]. Moreover, at high temperatures several diffusion mechanisms can be active, further complicating the scenario. Although the study of diffusion mechanisms is one of the classic problems in materials science, experimental probes of solid-state diffusion processes have so far been limited to macroscopic measurements of the time evolution of concentration profiles (commonly, tracer atoms or isotopes) [8–10]. The development of accurate quantum-mechanical calculations, based on density functional theory (DFT), along with advances in computing capabilities have improved the understanding of atomic-scale diffusion processes in a wide variety of materials [1,11–14]. To date, direct observations of atomic diffusion have been limited to the study of surface diffusion using scanning probe microscopes [3,7,15,16]. Direct imaging of bulk diffusion, which can be very different from surface diffusion mechanisms, has been lacking. Aberration-corrected scanning transmission electron microscopy (STEM) has already made possible the observation of single dopant atoms within nanowires [17] and bulk materials [18], including single jumps. Here, we show direct observation of extended diffusion of individual Ce and Mn atoms in wurtzite-type AlN (*w*-AlN) single crystals, tracking the impurities within the bulk material, and determine the pertinent mechanisms, including correlated steps, using aberration-corrected Z-contrast STEM imaging [19] (Z is the atomic number).

w-AlN doped with rare-earth or transition metals is a promising material for optoelectronic and magnetic applications [20]. Doping the technologically important class of group III nitrides, such as cubic boron nitride (*c*-BN) [21] and *w*-AlN [22], with large size-mismatch dopants has been successfully achieved by a reactive flux method operating at high pressures and high temperatures [23,24], which yields millimeter-size single crystals wherein single dopant atoms are uniformly dispersed and show homogeneous visible-light luminescence. However, the mechanisms by which the dopants are accommodated in the matrix are not fully understood and observation of the growth process *in situ* would be challenging. Therefore, to promote dopant diffusion in the solid and simulate a high-temperature condition without heating the specimen, we use a 200 kV electron beam, which provides sufficient energy for dopant migration but not enough to knock out the dopant atoms. We identify correlated vacancy-dopant diffusion to be the dominant mechanism in *w*-AlN followed by

 © 2014 American Physical Society

the less common interstitial kick-out mechanism [10]. We observe a number of jumps of the large-size Ce dopants in the *w*-AlN bulk, in agreement with the low migration energy barrier of 0.3–0.6 eV obtained by DFT calculations. On the basis of the DFT results, we elucidate the origin of this low migration energy barrier for the large-size Ce atoms to be the high formation energy of the Ce substitutional defects in the small *w*-AlN lattice and moreover we predict a higher barrier for a smaller atom, 2.1–2.6 eV for Mn. To confirm our theoretical prediction, we perform the same experiments for Mn doped *w*-AlN and find that the Mn atoms are indeed nearly stationary at the substitutional Al site.

When a specimen is exposed to a high-energy electron beam, the incident electron transfers energy to the constituent atoms. Assuming a purely elastic collision between a 200 kV electron and a stationary atom, the maximum energy transfer to Al and Ce atoms is estimated to be 18.2 and 3.5 eV, respectively (see Supplemental Material [25]). Although the maximum energy that can be transferred to the Ce atoms is large, it is considerably smaller than the calculated binding energy of a Ce atom present at a substitutional Al site, 13.4 eV. Thus, it is apparent that a 200 kV sub-Ångstrom electron beam is an optimum probe to both directly excite Ce dopants over the diffusion barrier at room temperature and observe events at the atomic scale, without directly knocking out dopants.

Figure 1 shows frames selected from a *Z*-contrast STEM image sequence of Ce-doped *w*-AlN viewed along the $[11\bar{2}0]$ direction with an acquisition time of 4 sec per frame (30 frames in total). The atomic "dumbbells" consisting of Al and N atoms are clearly resolved and the brighter columns are the Al sites [see the structural model in Fig. 1(h)]. The brightest column, indicated by arrowheads, contains a single Ce dopant [22], which moves to a different location in each panel. This sequence reveals that a single Ce dopant is moving in the bulk driven by the electron beam. Accurate quantification of the *Z*-contrast images using a recently developed technique [18] confirms that the dopant is inside the crystal rather than on the surface (see Supplemental Material [25]). We observe the Ce atom to have changed columns between frames on 11 occasions during the 30 frame sequence and the dopant trajectory is drawn on the frame-averaged image of Fig. 1(h). After the examination of the dopant trajectory, we can assign the Ce diffusion processes to three basic types: (1) basal-plane diffusion—(f) to (g) in frame 20, (2) pyramidal-plane diffusion—(b) to (c) in frame 5, and (3) interstitial-related diffusion—(f) and (g) in frame 16 and 20. In most cases (9 frames), the single Ce dopant jumps from a substitutional Al site into one of the nearest Al sites (basal- or pyramidal-plane diffusion) and then stays at the new substitutional Al site for a few frames prior to the next atomic jump. In two frames, (f) and (g) in Fig. 1, the Ce atom is located at interstitial sites (having moved either just as the beam approached or in the previous frame) and moves back to a substitutional Al site within the same frame. Over extensive observations of single Ce dopants, we did not identify *N*-site-related or direct interstitial diffusion steps (a direct atomic jump from one interstitial site to another interstitial site) in the

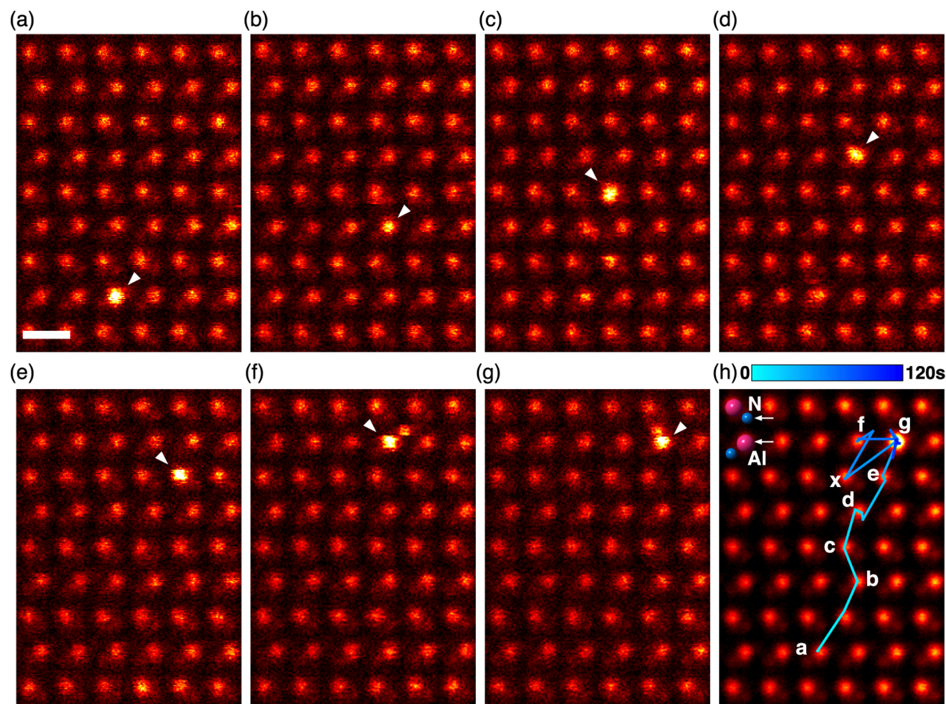

FIG. 1 (color online). Selected frames from a sequence of 30 *Z*-contrast images of a *w*-AlN single crystal doped with Ce viewed along the $[11\bar{2}0]$ axis. (a)–(g) Frames 1, 4, 5, 6, 10, 16, 20, respectively, show the locations of a single Ce dopant as marked by the arrowhead in each panel. (h) Frame-averaged *Z*-contrast image. The observed Ce trace is overlaid and the Ce positions in each panel (a)–(g) are indicated. The scale bar in (a) is 3 Å.

bulk. We construct more complicated or larger steps of single dopants inside *w*-AlN from combinations of the three basic types. For example, the observed diagonal atomic jump from the position x to g in Fig. 1(h) can be described as successive basal and pyramidal diffusion steps. Moreover, we frequently observed not purely random steps (Brownian motion) but *correlated* Ce dopant motion (see Supplemental Material [25]). In these cases, the Ce dopant rattles between two neighboring Al sites, in a manner characteristic of the vacancy-mediated diffusion mechanism proposed by Bardeen and Herring [26,27]. Thus, the microscopy results strongly suggest that we are seeing vacancy-, and occasionally, interstitial-mediated diffusion in Ce-doped *w*-AlN.

To better understand the energy landscape of Ce-doped *w*-AlN and calculate the activation energy for different Ce-diffusion mechanisms, we performed systematic first-principles calculations. We find a Ce atom substituting for Al (Ce_{Al}) to be the most stable configuration with a formation energy of 3.2 eV, in agreement with previous work [22,28]. We also find that the calculated activation energy for the concerted exchange [29] between Al and Ce atoms without any defects to be 8.0 and 10.0 eV for pyramidal-plane and basal-plane diffusion, respectively. These activation energies are higher than the energy transferred to the Ce atoms by the 200 kV incident electrons, and hence the concerted exchange mechanism is very unlikely. However, under our growth conditions, Al vacancies have a negative formation energy for *n*-type *w*-AlN and are therefore expected to form spontaneously during the crystal growth [22]. When the Ce dopant is coupled with a nearby Al vacancy, the activation energy for hopping is greatly reduced to 0.3 and 0.6 eV for basal-plane and pyramidal-plane diffusion, respectively [shown in Figs. 2(a), 2(b)]. Rather interestingly, the barrier for the migration of an Al atom to a vacancy site is noticeably higher at 2.5 eV. DFT calculated energies are known to have an error bar of 0.1 eV, or even larger for systems with strong correlations, such as Ce, so given that we do not often image the dopant at two sites in the same frame, the calculations probably underestimate the activation energies. Thus there remains an unresolved discrepancy between the experimental Ce hopping rate and the theoretical prediction (see Supplemental Material [25] for more details). Nevertheless, the calculated small barrier for a large-size Ce dopant, while striking, is in good agreement with the large number of jumps made by the Ce atom seen in our experiments, where we find it to move about every three frames. Under excitation by the electron beam, once a Ce dopant encounters an Al vacancy, the dopant readily jumps into the Al vacancy site. After a first vacancy-dopant exchange, the consecutive dopant jumps are no longer a pure random walk but a correlated walk with the Ce dopant trailing a leading Al vacancy. Strong evidence for this correlated dopant walk is provided by the experimentally observed back-and-forth Ce atom jumps (see Supplemental Material [25]) [12]. Although the energy barrier for the Al vacancy to migrate away from the Ce nearest neighbor position is high, it is possible under the beam excitation even at room temperature. Once the Al vacancy migrates away, the Ce atom awaits the arrival of the same or another Al vacancy in order to migrate to a different position. On the basis of both the experimental microscopy images and the theoretical calculations, we conclude that the observed basal- and pyramidal-plane diffusion is vacancy mediated, and the low theoretical energy barrier suggests that the vacancy-mediated diffusion mechanism can occur even at room temperature.

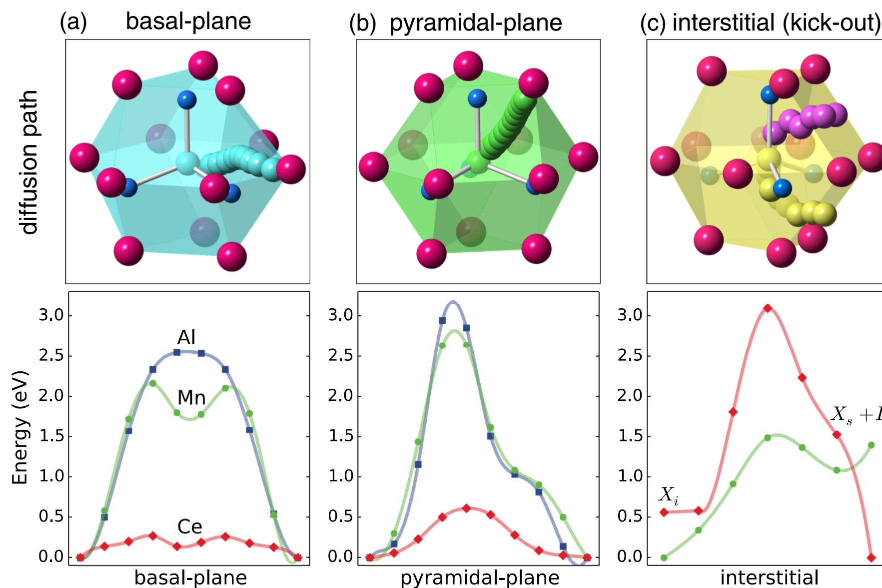

FIG. 2 (color online). The Ce dopant diffusion paths in *w*-AlN (top panels) and the diffusion energy surfaces (bottom panels). (a) Basal-plane diffusion (Al: red, N: blue, and Ce: light blue), (b) pyramidal-plane diffusion (Ce: light green), (c) interstitial diffusion with kick-out mechanism (Ce: yellow, Al interstitial: pink), with the interstitial dopant, substitutional dopant and self-interstitial defects labeled X_i, X_s, and I, respectively. The starting point is not at zero because an interstitial Al is more stable than an interstitial Ce.

As shown in Figs. 1(f) and 1(g), we also observed cases where the single Ce dopant moved into interstitial sites. We consider two well-known hybrid-type interstitial diffusion mechanisms, the Frank-Turnbull mechanism [30]: $V + X_i \rightleftarrows X_s$ and the kick-out mechanism [8]: $X_s + I \rightleftarrows X_i$ (V represents self-vacancy, I self-interstitial, X_s,substitutional dopant, X_i interstitial dopant). The absence of any deep local minima in the energy surfaces of the vacancy-mediated diffusion paths for Ce [Figs. 2(a) and 2(b)] makes it improbable that the dopant atom could occupy an interstitial site adjacent to an Al vacancy. Thus, the Frank-Turnbull mechanism [30] is unlikely in the present case. However, when the Ce dopant encounters an Al interstitial, the Ce dopant can move to the interstitial site through a kick-out mechanism. The energy surfaces for Ce dopants and the energy minimum diffusion path for Ce dopant based on the kick-out mechanism are shown in Fig. 2(c). Although the activation energy for Ce is high (3.1 eV), it is likely that the observed interstitial diffusion could be excited by the electron beam. Thus, it is also possible to study high-energy diffusion pathways that are inactive at room temperature, but can be active at higher temperatures and are known play an important role in failure mechanisms such as creep and fatigue [10]. This is an important advantage of using the electron beam to induce diffusion.

Even though the present calculations explain our observations well, the extremely small theoretical barrier for the vacancy-mediated Ce atom migration (lower than for an Al atom) raises further questions about the underlying migration mechanism and how it might be controlled. We calculated the activation energies for Ce dopant diffusion as a function of isotropic tensile stress applied to the w-AlN lattice that causes expansion of the host lattice. Figure 3 shows the activation energies for pyramidal diffusion of a Ce dopant as a function of volumetric strain, $(V - V_0)/V_0$ (V_0 is the volume per unit cell at zero tensile strain). In general, structural defects such as dislocations, grain boundaries, and free surfaces can enhance the diffusivity of a dopant because of their larger spaces and weakened chemical bonding. We thus expected that the expanded lattice would enhance the dopant diffusivity. However, the calculated results show the opposite behavior: lattice expansion around a Ce dopant leads to a higher activation energy, suggesting that a Ce substitutional defect becomes more stable in a larger space. This result can be explained by remembering that the Ce dopant is unusually large for the host lattice (size-mismatch) and the Ce substitutional defect has a high formation energy, even if coupled with a single Al vacancy [22]. As a result, the formation energy difference between the substitutional and the interstitial positions is reduced, and the Ce dopant becomes more mobile in the bulk, even at room temperature (without the electron beam). Conversely, our theoretical calculations predict that a smaller-size dopant such as Mn should have much smaller diffusivity, because the energy barriers for basal- and pyramidal-plane diffusion are calculated to be

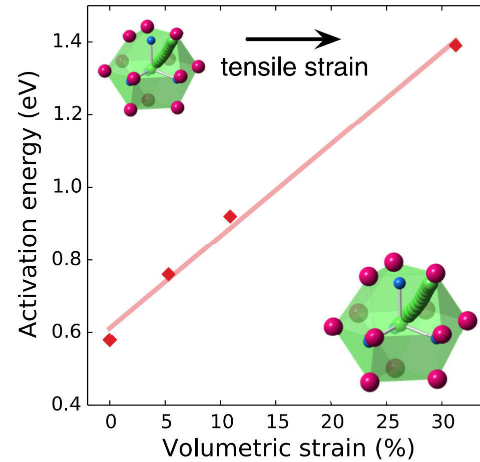

FIG. 3 (color online). Activation energies for Ce pyramidal-plane diffusion via the vacancy-mediated mechanism as a function of volumetric strain. The Ce diffusion barrier increases with increasing volume.

2.1 and 2.6 eV, which we attribute to the higher stability of the Mn substitutional defect (with a formation energy of 1 eV) compared to the Ce_{Al} defect (3.2 eV).

To test our prediction, we repeated our STEM experiments on Mn-doped w-AlN single crystals. In contrast to the Ce doped case, the Mn dopant has a lower atomic mass and the maximum transferred energy (9 eV) from an incident electron is much higher, suggesting that Mn should be more mobile than Ce in the bulk w-AlN. However, we typically observed zero or only a very few Mn atom jumps in 40–60 frames. Figures 4(a)–4(c) show typical atomic-resolution Z-contrast STEM images obtained from Mn doped w-AlN single crystals viewed along the $[11\bar{2}0]$, $[1\bar{1}00]$, and [0001] directions, with the corresponding structure models shown in Figs. 4(d)–4(f), respectively. These images are obtained by averaging over the sequentially acquired 40–60 frames and it can be seen that the Mn dopants stay at the specific Al sites. We further found that even after a Mn atom jump, the Mn dopant is basically stable at the new Al site. Thus, our observations confirm that the larger and heavier Ce dopants have a *higher* mobility than Mn dopants in w-AlN, in agreement with the theoretical predictions. On the basis of the theoretical activation energies (vacancy-mediated diffusion case), we estimate the dopant diffusion rates under the electron beam for Ce atoms to be more than 20 times higher than those for Mn atoms (see Supplemental Material [25]), which correlates well with the experimental observations.

In summary, we have visualized single Ce atom diffusion in w-AlN by time-sequential Z-contrast STEM imaging. The observed basal or pyramidal diffusion and interstitial-related diffusion for single Ce dopants are determined to be a vacancy-mediated mechanism and a kick-out mechanism, respectively, in good agreement with first-principles calculations. Our findings show how depth sensitive microscopy coupled with density functional calculations can be used to investigate the mechanisms and pathways

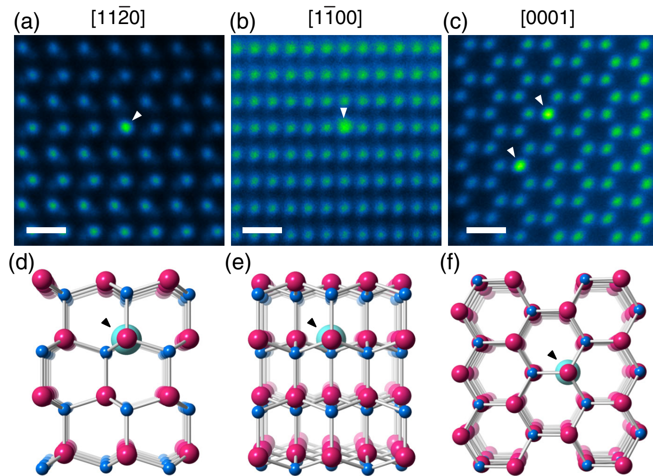

FIG. 4 (color online). Frame-averaged Z-contrast images of Mn-doped w-AlN single crystals. The brightest atomic columns in each panel are the location of single Mn dopants as marked by arrowheads in each panel. The scale bars are 3 Å. The crystal orientations are (a) [11$\bar{2}$0], (b) [1$\bar{1}$00], (c) [0001] with the corresponding structural models given in (d)–(f), respectively.

governing diffusion within bulk materials. In this case, the results show how dopant diffusivity may be enhanced by accommodating large-size dopants in a narrow space or at unstable atomic sites, or alternatively reduced by selecting smaller dopants. The methodology is applicable to many other systems, and may be useful to deliberately tailor materials for higher ionic conductivities or for longer device lifespans. Moreover, this method could be applicable to study diffusion mechanisms in other materials with barriers such that the transition times are comparable to the scan rate of the STEM.

R. I. acknowledges support from JSPS Postdoctoral Fellowship for research abroad. R. M. acknowledges support from U.S. DOE Grant No. DE-FG02-09ER46554. A. R. L, S. T. P. and S. J. P. acknowledge support by the U.S. DOE Office of Science, Basic Energy Sciences, Materials Sciences and Engineering Division. S. T. P. also acknowledges support by the McMinn Endowment at Vanderbilt University. S. D. F. acknowledges support under the Discovery Projects funding scheme of the Australian Research Council (Project No. DP110101570). R. I. and T. T. acknowledge support by a Grant-in-Aid for Scientific Research on Innovative Areas "Nano Informatics" (Grant No. 25106003) from JSPS. The research used resources of the National Energy Research Scientific Computing Center, which is supported by the Office of Science of the U.S. DOE under Contract No. DE-AC02-05CH11231.

R. I. and R. M. contributed equally to this work.

*To whom all correspondence should be addressed.
ishikawa@sigma.t.u-tokyo.ac.jp
†To whom all correspondence should be addressed.
rohan.mishra@vanderbilt.edu

[1] P. M. Fahey, P. B. Griffin, and J. D. Plummer, Rev. Mod. Phys. **61**, 289 (1989).
[2] H. Ohno, D. Chiba, F. Matsukura, T. Omiya, E. Abe, T. Dietl, Y. Ohno, and K. Ohtani, Nature (London) **408**, 944 (2000).
[3] N. Balke, S. Jesse, A. N. Morozovska, E. Eliseev, D. W. Chung, Y. Kim, L. Adamczyk, R. E. Garcia, N. Dudney, and S. V. Kalinin, Nat. Nanotechnol. **5**, 749 (2010).
[4] Y. Yamada, K. Ueno, T. Fukumura, H. T. Yuan, H. Shimotani, Y. Iwasa, L. Gu, S. Tsukimoto, Y. Ikuhara, and M. Kawasaki, Science **332**, 1065 (2011).
[5] V. C. Holmberg, J. R. Helps, K. A. Mkhoyan, and D. J. Norris, Chem. Mater. **25**, 1332 (2013).
[6] P. M. Koenraad and M. E. Flatté, Nat. Mater. **10**, 91 (2011).
[7] D. Gohlke, R. Mishra, O. D. Restrepo, D. Lee, W. Windl, and J. Gupta, Nano Lett. **13**, 2418 (2013).
[8] U. Gösele, W. Frank, and A. Seeger, Appl. Phys. A **23**, 361 (1980).
[9] U. Gösele and T. Y. Tan, Appl. Phys. A **28**, 79 (1982).
[10] H. Mehrer, *Diffusion in Solids* (Springer-Verlag, Heidelberg, 2007).
[11] R. Car, P. J. Kelly, A. Oshiyama, and S. T. Pantelides, Phys. Rev. Lett. **54**, 360 (1985).
[12] C. S. Nichols, C. G. Van de Walle, and S. T. Pantelides, Phys. Rev. Lett. **62**, 1049 (1989).
[13] P. E. Blöchl, C. G. Van de Walle, and S. T. Pantelides, Phys. Rev. Lett. **64**, 1401 (1990).
[14] M. Ramamoorthy and S. T. Pantelides, Phys. Rev. Lett. **76**, 267 (1996).
[15] R. M. Feenstra, A. J. Slavin, G. A. Held, and M. A. Lutz, Phys. Rev. Lett. **66**, 3257 (1991).
[16] S. Kitamura, T. Sato, and M. Iwatsuki, Nature (London) **351**, 215 (1991).
[17] S. H. Oh, K. Benthem, S. I. Molina, A. Y. Borisevich, W. Luo, P. Werner, N. D. Zakharov, D. Kumar, S. T. Pantelides, and S. J. Pennycook, Nano Lett. **8**, 1016 (2008).
[18] R. Ishikawa, A. R. Lupini, S. D. Findlay, T. Taniguchi, and S. J. Pennycook, Nano Lett. **14**, 1903 (2014).
[19] S. J. Pennycook and L. A. Boatner, Nature (London) **336**, 565 (1988).
[20] Y. Taniyasu, M. Kasu, and T. Makimoto, Nature (London) **441**, 325 (2006).
[21] R. Ishikawa, N. Shibata, F. Oba, T. Taniguchi, S. D. Findlay, I. Tanaka, and Y. Ikuhara, Phys. Rev. Lett. **110**, 065504 (2013).
[22] R. Ishikawa, A. R. Andrew, F. Oba, S. D. Findlay, N. Shibata, T. Taniguchi, K. Watanabe, H. Hayashi, T. Sakai, I. Tanaka, Y. Ikuhara, and S. J. Pennycook, Sci. Rep. **4**, 3778 (2014).
[23] T. Taniguchi and K. Watanabe, J. Cryst. Growth **303**, 525 (2007).
[24] T. Taniguchi and S. Yamaoka, J. Cryst. Growth **222**, 549 (2001).
[25] See Supplemental Material at http://link.aps.org/supplemental/10.1103/PhysRevLett.113.155501 for additional data, details of experimental and DFT calculation procedures, and supplementary discussion.
[26] J. Bardeen and C. Herring, *Atom Movements* (A.S.M., Cleveland, 1951).
[27] J. Bardeen and C. Herring, *Imperfections in Nearly Perfect Solids* (Wiley, New York, 1952).
[28] The formation energies are calculated for the neutral defects under N-rich conditions.
[29] K. C. Pandey, Phys. Rev. Lett. **57**, 2287 (1986).
[30] F. C. Frank and D. Turnbull, Phys. Rev. **104**, 617 (1956).